AD-A130 183 A NUMERICAL METHOD IN SOLVING A COUPLED THERMOELASTICITY EQUATION AND SOME RESULTS(U) RUTGERS - THE STATE UNIV PISCATAWAY NJ Y Y LI ET AL. 10 JUN 83 1/1

UNCLASSIFIED DAAK10-81-C-0040 F/G 12/1 NL

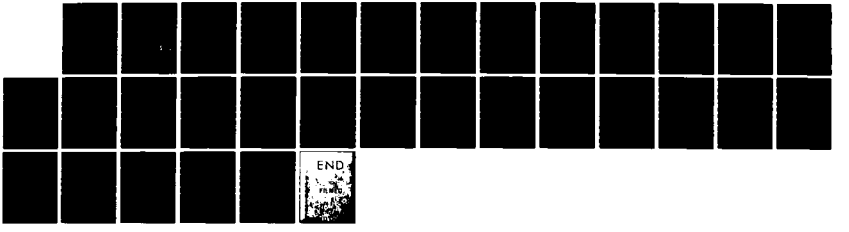

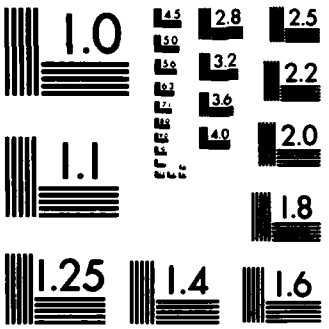

MICROCOPY RESOLUTION TEST CHART
NATIONAL BUREAU OF STANDARDS-1963-A

SECURITY CLASSIFICATION OF THIS PAGE (When Data Entered)

(12)

REPORT DOCUMENTATION PAGE		READ INSTRUCTIONS BEFORE COMPLETING FORM
1. REPORT NUMBER	2. GOVT ACCESSION NO. AD-A130183	3. RECIPIENT'S CATALOG NUMBER
4. TITLE (and Subtitle) A Numerical Method in Solving a Coupled Thermoelasticity Equation and Some Results		5. TYPE OF REPORT & PERIOD COVERED Final, June 1983
		6. PERFORMING ORG. REPORT NUMBER
7. AUTHOR(s) Y.Y. Li, H. Ghoneim, Y. Chen, J. Davis		8. CONTRACT OR GRANT NUMBER(s) DAAK10-81-C-0040
9. PERFORMING ORGANIZATION NAME AND ADDRESS Rutgers-The State University of New Jersey P.O. Box 909 Piscataway, NJ 08854		10. PROGRAM ELEMENT, PROJECT, TASK AREA & WORK UNIT NUMBERS
11. CONTROLLING OFFICE NAME AND ADDRESS DCASMA Springfield 240 Route 22 Springfield, NJ 07081		12. REPORT DATE June 10, 1983
		13. NUMBER OF PAGES 30
14. MONITORING AGENCY NAME & ADDRESS(if different from Controlling Office) Mr. Julian Davis Fire Control & Small Caliber Weapons System Lab ARRADCOM Dover, N.J.		15. SECURITY CLASS. (of this report) Unclassified
		15a. DECLASSIFICATION/DOWNGRADING SCHEDULE

16. DISTRIBUTION STATEMENT (of this Report)

The view, opinions, and/or findings contained in this report are those of the authors and should not be construed as an official Department of the Army position, policy or decision, unless so designated by other documentation.

This document has been approved for public release and sale; its distribution is unlimited.

17. DISTRIBUTION STATEMENT (of the abstract entered in Block 20, if different from Report)

DTIC ELECTE JUL 8 1983 S D A

18. SUPPLEMENTARY NOTES

19. KEY WORDS (Continue on reverse side if necessary and identify by block number)

Thermal Stress in Gun Barrel, Coupled Thermoelasticity Equation

20. ABSTRACT (Continue on reverse side if necessary and identify by block number)

This report discusses a numerical method in solving a coupled dynamical thermoelasticity problem in a long hollow cylinder. The inner boundary conditions are the traction and the fluid temperature imposed on the inner surface of the cylinder, whereas the outer boundary is subjected to the ambient fluid temperature and is free of traction. This problem is solved by a finite element method in which the spatial and the time variables are discretized by several schemes. The study shows that the central explicit scheme for space

(continued)

DD FORM 1 JAN 73 1473 EDITION OF 1 NOV 65 IS OBSOLETE

discretization combined with a time marching scheme which incorporates moderate damping is suitable for this particular problem.

Numerical results of the temperature and stress responses due to a modified step or single pulse are presented and discussed. One interesting observation is that, under high rate of stress loading, the coupling in the energy equation could generate temperature variations of significant magnitude.

1. Introduction

Early investigations on thermo-mechanical interaction resulted in the classical studies of thermoelasticity. Two major treatises have been published which summarize the contributions in thermoelasticity up to the time of early nineteen sixties [1-2]. Most commonly, problems of thermal stress were formulated such that the temperature field does not depend on the stress field, whereas the stress field is affected by the thermal expansion or contraction of the material. However, the fully coupled system of equations of thermoelasticity containing coupling terms in both the equation of motion and the energy balance equation has received relatively little effort until more recently. This development is largely due to the fact that these equations by and large are not easily accessible by the available analytical techniques. Some successes were achieved in isolated cases [3-5]. In these cases several methods of analysis including Laplace transform or perturbation series have been employed. For the fully coupled equations with arbitrary coupling coefficient and with general type of boundary conditions one must resort to numerical techniques. Numerical approach to the solution of the fully coupled thermoelasticity equation has appeared in the literature [6]. More recently, finite element method has been applied in solving the boundary value problem in a slab [7]. Results of the analysis of the slab indicate that under high rate of loading the coupling term in the energy balance equation should not be ignored.

This paper presents the numerical method and some results obtained in solving the coupled dynamical thermoelasticity equations in a long hollow cylinder, subjected to the pressure and the heat flux boundary conditions at the inner surface and ambient environment at the outer surface by a finite

element method. Several numerical schemes are studied for comparison purpose. Besides exhibiting the physics of the problem, this paper also is intended to show how various numerical schemes are suited for these problems.

2. Mathematical Model

The classical coupled dynamical thermoelasticity equations are a pair partial differential equations governing the balance of the linear momentum and the energy as given by the following [2].

$$\mu\nabla^2\underset{\sim}{u} + (\lambda + \mu)\ \text{grad div}\ \underset{\sim}{u} + \underset{\sim}{F} - \gamma\ \text{grad}\ T = \rho\ddot{\underset{\sim}{u}} \tag{1}$$

and

$$\nabla^2 T - \frac{1}{k}\dot{T} - \eta\ \text{div}\ \dot{\underset{\sim}{u}} = -\frac{Q}{k} \tag{2}$$

where $\underset{\sim}{u}$ is the displacement vector and T is the temperature, λ and μ are Lame's constants, ρ is the density, k is the diffusivity, Q is the heat source, γ and η are defined as:

$$\gamma = (3\lambda + 2\mu)\alpha^*$$
$$\eta = \gamma T_o/\rho c k \tag{3}$$

where α^* is the coefficient of thermal expansion, c is the heat capacity, T_o is the ambient temperature.

For a cylinder, the pair of equations (1) and (2) reduces to

$$-\frac{1}{r}\frac{\partial}{\partial r}\left(r\frac{\partial u}{\partial r}\right) + \frac{u}{r^2} + \frac{\ddot{u}}{c_1^2} + m\frac{\partial T}{\partial r} = 0 \tag{4}$$

and

$$-\frac{1}{r}\frac{\partial}{\partial r}\left(r\frac{\partial T}{\partial r}\right) + \frac{1}{k}\dot{T} + \eta\frac{1}{r}\frac{\partial}{\partial r}(r\dot{u}) = 0 \tag{5}$$

Notice that due to polar symmetry the displacement vector $\underset{\sim}{u}$ is reduced to the radial displacement u, whereas the tangential component is identically zero. Also, it is assumed that $\underset{\sim}{F} \equiv 0$, $Q \equiv 0$.

In Eqs. (4) and (5), we have

$$m = \gamma/(2\mu + \lambda) \quad \text{and} \quad c_1^2 = (\lambda + 2\mu)/\rho \tag{6}$$

The initial conditions on u and T are: $u(r,0)=0$, $T(r,0)=0$.

The boundary conditions are:

at the inner boundary, $r = r_i$

$$(\lambda + 2\mu)\frac{\partial u}{\partial r} + \lambda \frac{u}{r} - \gamma(T - T_o) - f^*(t) = 0$$

and (7)

$$\frac{\partial T}{\partial r} - \beta_1^* [T - g^*(t)] = 0$$

at the outer boundary, $r = r_o$

$$(\lambda + 2\mu)\frac{\partial u}{\partial r} + \lambda\frac{u}{r} - \gamma(T - T_o) = 0$$

and (8)

$$\frac{\partial T}{\partial r} + \beta_2^* T = 0$$

where $\beta_1^* = h_1/K$ and $\beta_2^* = h_2/K$, h_1 and h_2 are the heat transfer coefficients at the inner and outer boundaries respectively. K is the thermal conductivity.

It is noted that the data on the forcing functions f* and g* are compatible in that both these functions are continuous at the initial time.

Introducing the following set of non-dimensional variables

$$\bar{T} = \frac{T - T_o}{T_o} \quad , \quad \bar{r} = \frac{r}{r_i} \quad , \quad \tau = \frac{c_1 t}{r_i} \quad \text{and} \quad \bar{u} = \frac{u}{r_i} \tag{9}$$

and after some algebra, Eqs. (4) and (5) are transformed into the following non-dimensional equations with bars removed.

$$- \frac{\partial}{\partial r}(r\frac{\partial u}{\partial r}) + \frac{u}{r} + r\ddot{u} + \lambda_2 \, r\frac{\partial T}{\partial r} = 0 \tag{10}$$

and

$$- \frac{\partial}{\partial r}(r\frac{\partial T}{\partial r}) + \bar{c} \, r \, \dot{T} + \bar{c} \, \lambda_1 \frac{\partial}{\partial r} (r\dot{u}) = 0 \tag{11}$$

where $\bar{c} = c_1 r_i/k$, $\lambda_1 = k\eta/T_o$ and $\lambda_2 = mT_o$.

The initial conditions are: $u(r,0)=0$, $T(r,0)=0$ and the boundary conditions are: at the inner boundary, $r = 1$

$$\frac{\partial u}{\partial r} + \alpha \frac{u}{r} - \lambda_2 T - f(\tau) = 0$$

$$\frac{\partial T}{\partial r} - \beta_1 T + \beta_1 g(\tau) = 0 \tag{12}$$

at the outer boundary, $r = r_o$

$$\frac{\partial u}{\partial r} + \alpha \frac{u}{r} - \lambda_2 T = 0$$

$$\frac{\partial T}{\partial r} + \beta_2 T = 0 \tag{13}$$

where $\beta_1 = \beta_1^* r_i$, $\beta_2 = \beta_2^* r_i$, $\alpha = \lambda/(2\mu + \lambda)$,

$g(\tau) = [g^*(t) - T_o]/T_o$ and $f(\tau) = f^*(t)/(\lambda + 2\mu)$.

3. SPACE DISCRETIZATION

Two approaches are used in the space discretization - Galerkin method which uses linear shape function and generates consistent mass and conductivity matrices, and central explicit method which uses quadratic shape functions and generates lumped mass and conductivity matrices.

3.1 Galerkin Method. In this method it is assumed that both of the approximate solutions of Eqs. (10) and (11), $\tilde{u}$ and $\tilde{T}$ respectively, can be expanded in terms of the same shape function $\psi_i(r)$ (Figure 1).

$$\tilde{u} = \sum_{i=0}^{n} \psi_i(r) u_i(\tau)$$

$$\tilde{T} = \sum_{i=0}^{n} \psi_i(r) T_i(\tau) \qquad (14)$$

where n is the number of nodes, including the two boundary nodes. u_i and T_i are the approximate nodal values of the displacement and the temperature respectively.

Substituting Eq. (14) into Eqs. (10), (11), and (12) and (13) and imposing the condition

$$\int_{r_i}^{r_o} R_k \psi_j(r) dr = 0 \qquad j = 0,1,2,\text{----}n \quad , \quad k = 1,2 \qquad (15)$$

where R_1 and R_2 are the residues calculated upon substitution as stated, and performing integration and some algebraic work lead to the following pair of linear algebraic equations:

$$[MU2]\ddot{\underline{U}} + [KU2]\underline{U} + \lambda_2[KT2]\underline{T} = \underline{F}^{(2)} \tag{16}$$

and

$$[CT1]\dot{\underline{T}} + \frac{1}{\bar{C}}[KT1]\underline{T} + \lambda_1[CU1]\dot{\underline{U}} = \underline{F}^{(1)} \tag{17}$$

where [MU2], [KU2],----, etc. are tridiagonal N x N matrices. The details of deriving the solution given in Eqs. (15), (16) and (17) can be found in Appendix A.

3.2 Central Explicit Method. In this case the shape functions $\psi_i(r)$ are quadratic instead of linear. The weighting function is taken to be $\delta(r-r_i)$. We let $\tilde{u}$ and $\tilde{T}$ be the following quadratic expansion within each element.

$$\tilde{u} = \sum_{i-1}^{i+1} \psi_i(r)\ u_i(\tau)$$

$$\tilde{T} = \sum_{i-1}^{i+1} \psi_i(r)\ T_i(\tau) \tag{18}$$

where the ψ's are the Lagrange polynomials.

Figure 2 illustrates the ψ-function.

Using the same notation as before, we impose the condition

$$\int_{i-1}^{i+1} R_j\ \delta(r-r_i)dr = 0\ , \qquad \begin{matrix} i = 0,1,2,---n \\ j = 1,2 \end{matrix} \tag{19}$$

The respective coefficient matrices of Eqs. (16) and (17) for this procedure are given in Appendix B.

4. TIME MARCHING

Two approaches have been tried: the general implicit scheme [8] and the three-point recurrence scheme [9].

4.1 General Implicit Method (GIM). For convenience we shall write Eqs. (16) and (17) in a single equation

$$\underline{M}\ddot{\underline{X}} + \underline{C}\dot{\underline{X}} + \underline{K}\underline{X} = \underline{F} \tag{20}$$

where $\underline{X} = \{\underline{u}, \underline{T}\}^T$

$$\underline{M} = \begin{bmatrix} MU2 & 0 \\ 0 & 0 \end{bmatrix}$$

$$\underline{K} = \begin{bmatrix} KU2 & \lambda_2 KT2 \\ 0 & \frac{1}{c} KT1 \end{bmatrix}$$

$$\underline{C} = \begin{bmatrix} 0 & 0 \\ \lambda_1 CU1 & CT1 \end{bmatrix}$$

$$\underline{F} = \{\underline{F}^{(2)} \; ; \; \underline{F}^{(1)}\}$$

Equation (20) can be written as a first order differential equation in the form

$$\underline{A}\dot{\underline{Y}} = \underline{B}\underline{Y} + \underline{F} \tag{21}$$

where $\underline{Y} = \{\dot{\underline{U}}\ \underline{U}\ \underline{T}\}^T$

$$\underline{F} = \{\underline{F}^{(2)}\ \underline{0}\ \underline{F}^{(1)}\}^T$$

$$A = \begin{bmatrix} MU2 & 0 & 0 \\ 0 & I & 0 \\ 0 & 0 & CT1 \end{bmatrix}$$

$$B = \begin{bmatrix} 0 & -KU2 & -\lambda_2 KT2 \\ I & 0 & 0 \\ -\lambda_1 CU1 & 0 & -\frac{1}{c} KT1 \end{bmatrix}$$

Applying GIM to Eq. (21) we obtain the following two-point recurrence scheme

$$[A-\Delta\tau\theta B]\underline{Y}^{i+1} = [A+\Delta\tau(1-\theta)B]\underline{Y}^{i} + \Delta\tau[\theta\underline{F}^{i+1} + (1-\theta)\underline{F}^{i}] \qquad (22)$$

where θ is a parameter, $0 \leq \theta \leq 1$.

The selection of the value of θ depends on the problem on hand, guided by the stability, accuracy and economy of the computation. The value $\theta = 0.667$ has been shown to be a good choice [9,10].

4.2 Three-Point Recurrence Method (GFE)

Let the shape function $N_i(\tau)$ be defined such that

$$N_{i-1}(\tau) = -\xi(1-\xi)/2$$

$$N_i(\tau) = (1-\xi)(1+\xi) \qquad (23)$$

$$N_{i+1}(\tau) = \xi(1+\xi)/2$$

where $\xi = \tau/\Delta\tau$

Figure 3 illustrates the $N_i(\tau)$ functions.

$$\text{Let} \quad \underset{\sim}{\bar{X}}(\tau) = N_{i-1}(\tau)\underset{\sim}{X}_{i-1} + N_i(\tau)\underset{\sim}{X}_i + N_{i+1}(\tau)\underset{\sim}{X}_{i+1} \tag{24}$$

The residue R is defined as

$$R = M\,\underset{\sim}{\ddot{\bar{X}}} + C\,\underset{\sim}{\dot{\bar{X}}} + K\,\underset{\sim}{\bar{X}} - \underset{\sim}{F} \tag{25}$$

We require that

$$\int_{i-1}^{i+1} R\, W_i(\tau)\, d\tau = 0 \tag{26}$$

where $W_i(\tau)$ is the weighting function. Performing the operation in Eq. (26) yields

$$[M + \gamma\Delta\tau C + \beta\Delta\tau^2 K]\underset{\sim}{X}_{i+1} + [-2M + (1-2\gamma)\Delta\tau C$$

$$+ (\tfrac{1}{2} - 2\beta + \gamma)\Delta\tau^2 K]\underset{\sim}{X}_i + [M - (1-\gamma)\Delta\tau C + (\tfrac{1}{2} + \beta - \gamma)\Delta\tau^2 K]\underset{\sim}{X}_{i-1}$$

$$- \underset{\sim}{F}\Delta\tau^2 = 0 \tag{27}$$

where β and γ are two parameters depending on the weighting function chosen.

$$\beta = \int_{-1}^{1} W_i(\xi)\, \frac{\xi(1+\xi)}{2}\, d\xi \Big/ \int_{-1}^{1} W_i(\xi)\, d\xi$$

and

$$\gamma = \int_{-1}^{1} W_i(\xi)\,(\xi + \tfrac{1}{2})\, d\xi \Big/ \int_{-1}^{1} W_i(\xi)\, d\xi$$

lect of various combinations of β and γ for the solution of problems
amics has been studied [11].

AND DISCUSSION

here are two schemes each for the space and the time discretization,
the time discretization schemes there are several choices of values of
ers θ , β and γ, many combinations of the space and time discretizations
e for the numerical solution of the physical problem.
oblems were selected with a view to compare the results of computation
g the relative merit of each scheme regarding the stability and

sponses to a Modified Step Stress Input (Wave Equation Only).

e first series of computation was done to test the wave propagation
When the temperature T was removed by putting $\lambda_1 = \lambda_2 = 0$ and
boundary condition deleted, the remaining system of equations
a wave equation, for which analytical solution exists.
te computation a modified step stress is given as

$$f(\tau) = -0.1(1 - e^{-10\tau})$$

owing computation the same time and spatial increments are used for all.

ersus τ Responses

- Figure 4 shows the result of computation using Galerkin (GK) in
IM in time discretization. Three different values of θ were used:
ntral difference), $\theta = 0.667$ (Gelerkin) and $\theta = 1$ (backward). The

figure shows the radial and tangential stresses versus time at the midpoint ($r = 1.45$). The results indicate that in the case of $\theta = 0.667$, least amount of spurious oscillation exists, whereas the other two schemes of GIM lead to either spurious oscillation or excessive damping as evidenced by the drastic reduction in amplitude.

GK/GFE - Figure 5 is the same set of responses calculated by GK/GFE with four different sets of values for β and γ. They are (1) $\beta = 0.25$, $\gamma = .5$ (2) $\beta = 1/6$, $\gamma = .5$, (3) $\beta = .5$, $\gamma = .6$, (4) $\beta = .8$, $\gamma = 1.5$. Results show that the third set of β and γ give neither spurious oscillation nor excessive damping.

CD/GIM or GFE - Figure 6 shows the computation based on a central explicit (CD) scheme in space and three different schemes in time (1) GIM, $\theta = 0.667$ (2) GFE, $\beta = .5$, $\gamma = .6$ and (3) GFE, $\beta = .8$, $\gamma = 1.0$.

Curve (1) shows comparatively little dissipation in the amplitude responses, whereas curve (2) and (3) exhibit significant dissipation.

In summary, it is demonstrated that several schemes give comparable results in the wave propagation responses which are accurate and stable, as can be verified at least qualitatively by a method such as characteristics. In the following, the fully coupled fields in the cylinder are analyzed subject to either stress or thermal inputs at the inner bore. In the stress input we use both pulse or step type input, whereas only pulse type input is used for the temperature.

In this paper it is not the intention to give details regarding the physical problem involved. The parameters used in the calculation derive their origin from the application problem. For reference purposes, a list of the values of the parameters used in the computation is given.

The amplitudes of the pulses and the step are realistic values corresponding to the physical situation in the application.

5.2 Responses to a single stress pulse, $f(\tau) = -0.015\tau e^{-2\tau}$ for different r_o/r_i - $\Delta\tau/\Delta\gamma$ - and θ - values (fully coupled equations).

The next series of three figures show the radial stress versus time responses of the cylinder with fully coupled equations subject to a single stress pulse. Figure 7 shows for a cylinder with $r_o/r_i = 2.0$. Curve (1), (3) and (4) correspond to GIM with different values of θ. From these curves it appears that when $\theta = 0.667$ as shown in curve (1) the result is the best. Curve (3) with $\theta = 0.5$ shows too much oscillation, and curve (4) with $\theta = 1.0$ shows significant "numerical dissipation".

Curve (1) and (2) have the same θ-value but different $\Delta\tau/\Delta\gamma$. Curve (1) with $\Delta\tau/\Delta\gamma = 0.2$ gives better result in that it has less "numerical dissipation".

Figure 8 is a similar computation but with $\mu_o/\mu_i = 1.5$, $\theta = 0.667$, but different $\Delta\tau/\Delta\gamma$. Curve (3) uses a very small $\Delta\tau(= 0.002)$, thus requires too much computation time. Curve (2) exhibits significant "numerical dissipation". Curve (1) with $\Delta\tau/\Delta\gamma = 0.2$ is the best compromise.

Figure 9 is calculation for a very thin cylinder with $\gamma_o/\gamma_i = 1.1$. The schemes use $\theta = 0.667$ and $\Delta\tau/\Delta\gamma = 0.2$ and 2.0 respectively. For $\Delta\tau/\Delta\gamma = 0.2$ the result shows less dissipation, whereas for $\Delta\tau/\Delta\gamma = 2.0$ the result shows significant "numerical dissipation".

Therefore, from the above results we chose $\theta = 0.667$, $\Delta\tau/\Delta\gamma = 0.2$ for computing responses to stress inputs.

5.3 Responses to a Modified Step Stress, $f(\tau) = -.003(1-e^{-10\tau})$

Figure 10 shows the responses in the radial stress, tangential stress and temperature versus time. For the given input the rise time is 0.8, i.e. when $\tau=0.8$, $f(\tau) = -.003$. The plot is for the midpoint between the fifth and the sixth nodes with the non-dimensional $r=1.45$. Since the non-dimensional time τ is scaled against the travel time of the elastic wave through a distance equal to the inner radius and the non-dimensional distance is scaled against the length equal to the inner radius, it would take a unity of time for the radial wave to travel a unit distance in non-dimensional scales. Thus, the time of arrival of the radial wave should be about $\tau \approx 0.45$. This is indeed the case as shown in Fig. 10. Notice that the radial wave does not rise to the maximum value of the input as it would be the case in a slab [7], due to the effect of the curvature. Observed is also the fact that the reflected wave, being tensile in nature due to the free surface at the outer boundary, gives rise to intervals of time when the radial stress drops off and becomes tensile stress for a short time. A periodicity of $\tau=2$ is observed from the figure with good regularity within the time plot. The travel time of the tangential wave should be about $(2\pi)(1.45)/1$ or 9.11. The calculation gives a good approximate check.

The temperature response in the cylinder is due to the coupling in both field equations. Predictably, the temperature generated is small, about $0.6°C \sim -1.4°C$ referred to ambient when the ambient temperature is 27°C. It can be either positive or negative corresponding to a rise on a drop from the ambient temperature due to a volumetric compression or expansion. This effect usually is very small. Here, due to the high rate of change of strain, the coupling effect is not ignorable.

5.4 Responses to a Single Triangular Stress Pulse

A triangular pressure pulse of duration equal to 2 and amplitude equal to 0.003 is applied at the inner boundary. Figure 11 shows the responses vs time and Figure 12 the distribution of responses.

For large time τ a standing-wave like motion is observed in Figure 12 as each point goes through a periodic motion of different amplitude, whereas the two boundaries in this case are both traction free after $\tau=2$.

After $\tau=2$, the maximum non-dimensional radial stress occurring at $\tau=2.4$ is tensile in nature and equals to 0.00194. The corresponding minimum is a compressive stress .00164 at $\tau=7.4$. The induced temperature varies from 1.2°C at $\tau=7.4$ to -1.3°C at $\tau=2.4$, referred to the ambient temperature. The variation is about ±5% of the ambient temperature. These responses are not graphed in the figures shown.

5.5 Response to a Temperature Pulse, $g(\tau) = 0.008155\tau e^{-0.0005\tau}$

The time scale for the temperature response is about four decades longer than the stress response. The responses are evaluated at times when $\tau \sim 10^4$. In the numerical computation a time increment was chosen with the same factor in mind.

Figures 13 and 14 show the radial and tangential stress distribution for various times. Notice that when τ is 10^4 the physical time t is 0.173 sec. From $\bar{\tau} = 0.2$ to $\bar{\tau} = 0.5$ the actual time elapsed is 0.0519 sec., a relatively short time for heat transfer.

The maximum temperature is 0.124 (~64.2°C) at the inner surface when $\tau = 1.2 \times 10^4$. It drops down quickly as shown in Figure 15.

6. Summary

In summary, several observations can be made from the results of the numerical experiments of this investigation.

(1) It is possible through deliberate experimentation to arrive at a feasible numerical scheme to limit the amount of numerical dispersion and dissipation to a reasonable level.

(2) The coupling introduced in the energy equation could cause temperature fluctuation due to a rapidly applied stress input in the order of 5 to 10% for a single pulse input, depending on the rate of application.

(3) The effect of the curvature is to decrease the peak response of the radial stress, in the presence of the tangential stress component.

ACKNOWLEDGEMENT

This work is sponsored by ARRADCOM, Dover, New Jersey under contract DA-0040.

References

1. Boley, B. A. and Weiner, J. H., Theory of Thermal Stresses, Wiley, 1960.

2. Nowacki, W., Thermoelasticity, Addison-Wesley, 1962.

3. Dillon, O. W., Thermoelasticity when the Material Coupling Parameter Equals Unity, J. Appl. Mech., Vol. 32, No. 2, 1965, pp. 378-382.

4. Soler, A. I., Brull, M. A., On the Solution to Transient Coupled Thermoelastic Problems by Perturbation Techniques, J. Appl. Mech., Vol. 32, No. 2, 1965, pp. 389-399.

5. Achenbach, J. D., Approximate Transient Solutions for the Coupled Equations of Thermoelasticity, J. Acoust. Soc., Vol. 36, No. 1, 1964, pp. 10-18.

6. Oden, T. J., Finite Elements of Nonlinear Continua, McGraw-Hill, 1972.

7. Chen, Y., Ghoneim, H., Davis, J., A Finite Element Solution of the Coupled Thermoelasticity Equations in a Slab, Advances in Computer Technology, ASME, Vol. 2, 1980, pp. 199-218.

8. Richtmeyer, R. D., Morton, K. W., Difference Method for Initial-Value Problems, 2nd Ed., Wiley, N.Y., 1967.

9. Zamal, M., The Mathematics of Finite Element and Applications II, Academic Press, 1975, pp. 85-104.

10. Zienkiewicz, O. E., The Finite Element Method, Third Ed., McGraw-Hill, 1977, pp. 570-574.

11. Goudreau, G. L., Taylor, R. L., Evaluation of Numerical Integration Methods in Elastodynamics, Comp. Method. Appl. Mech., Eng., Vol. 2, 1972, pp. 69-97.

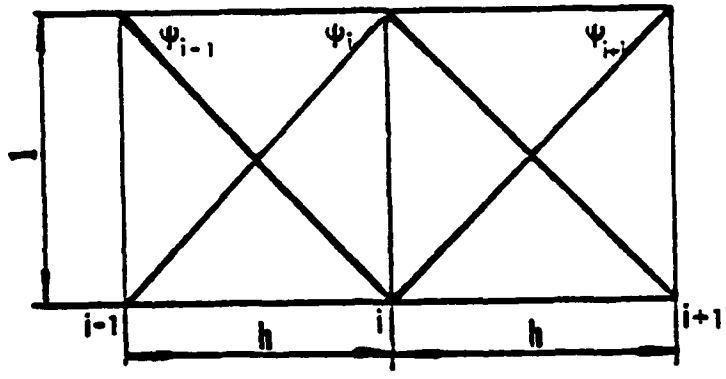

FIG. 1 GALERKIN

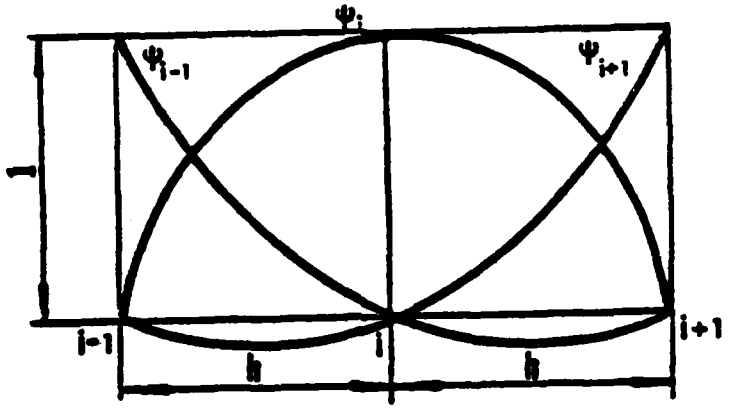

FIG. 2 CENTRAL DIFFERENCE

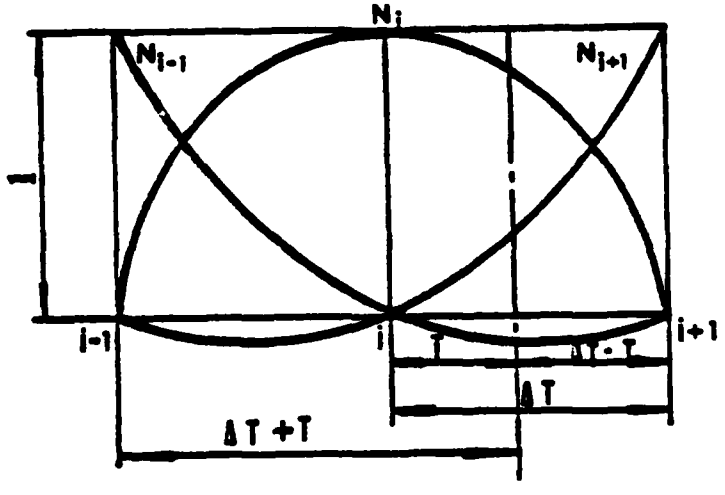

FIG. 3 GFE

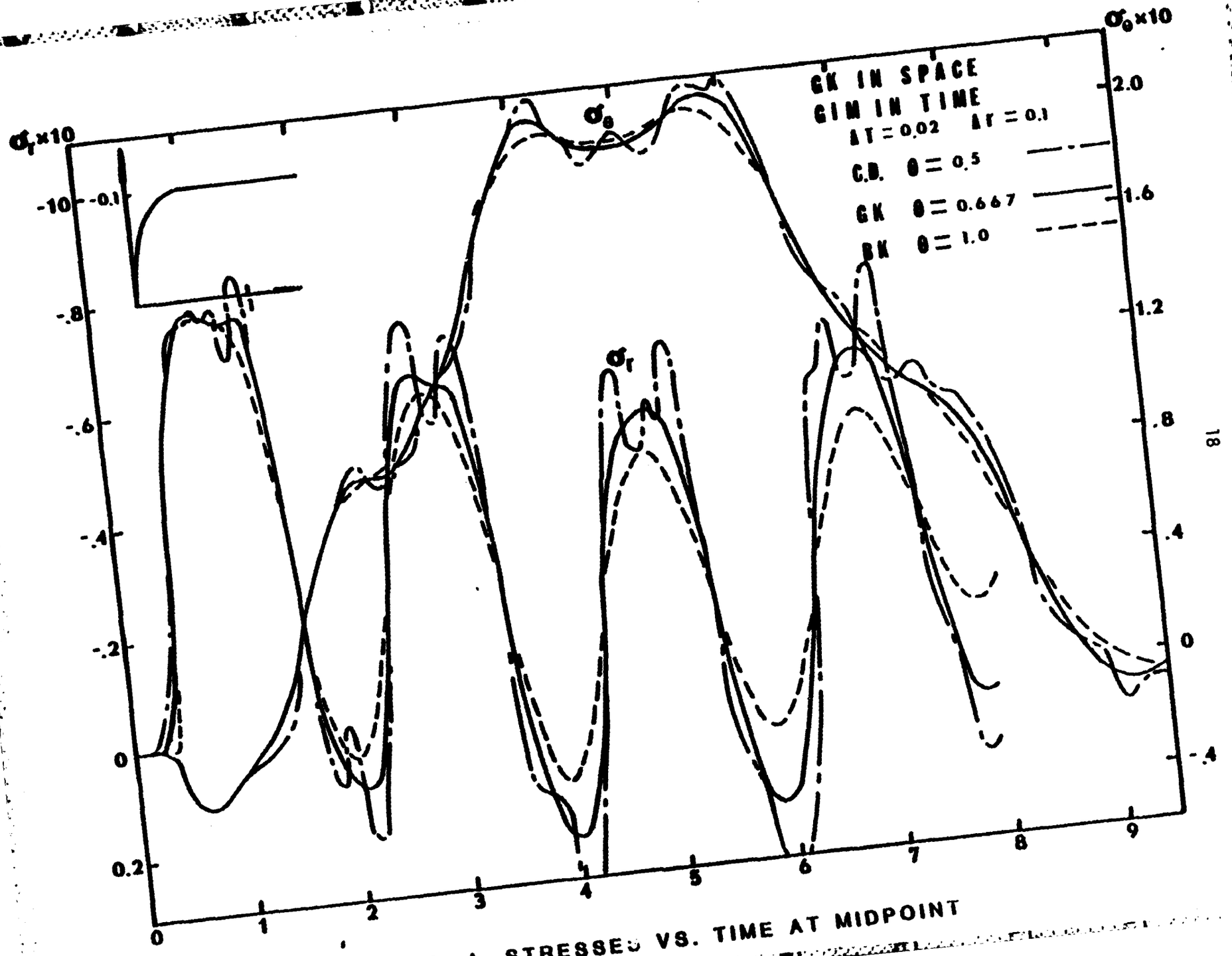

FIG. 4 STRESSES VS. TIME AT MIDPOINT

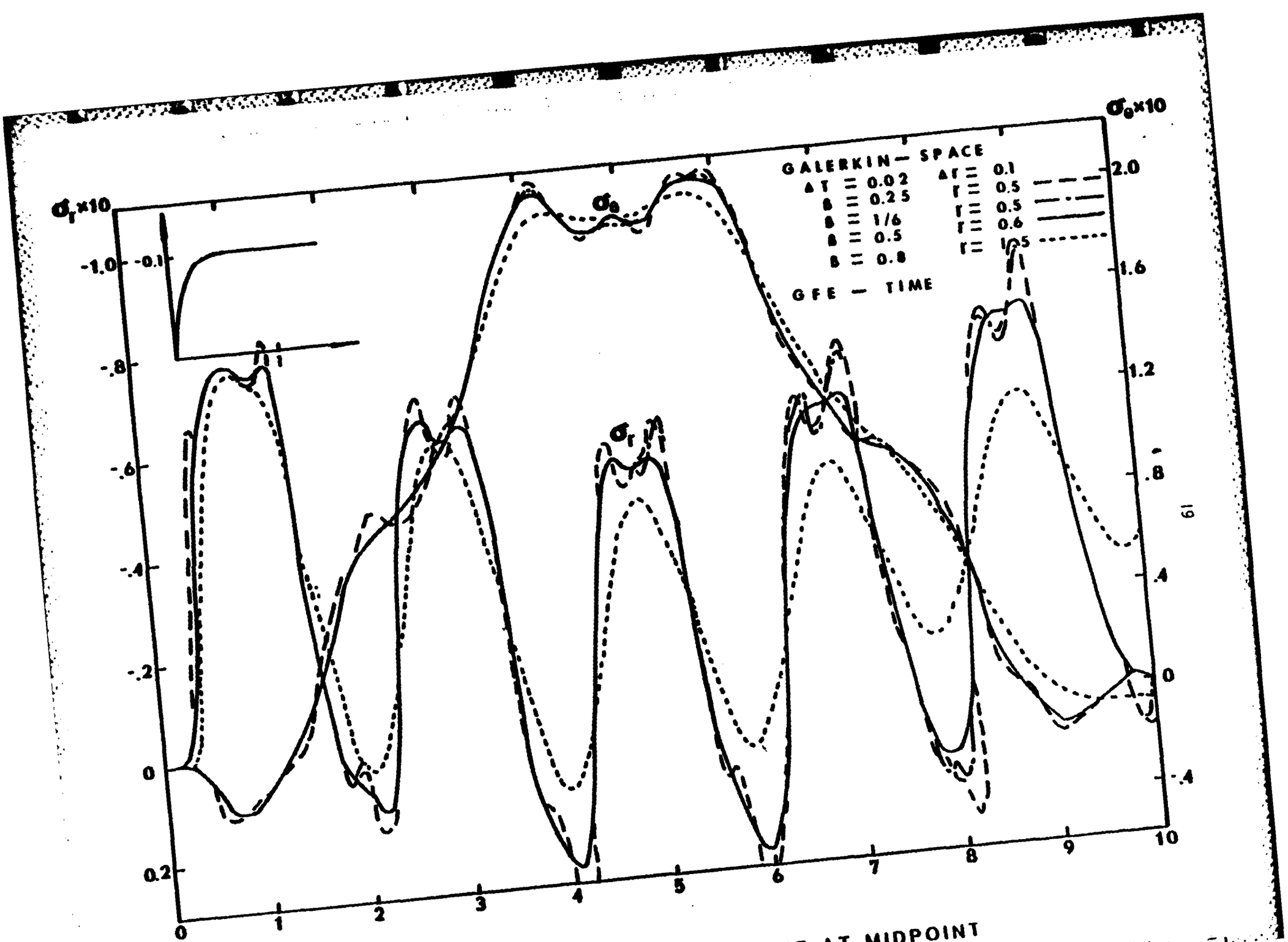

FIG. 5 STRESSES VS. TIME AT MIDPOINT

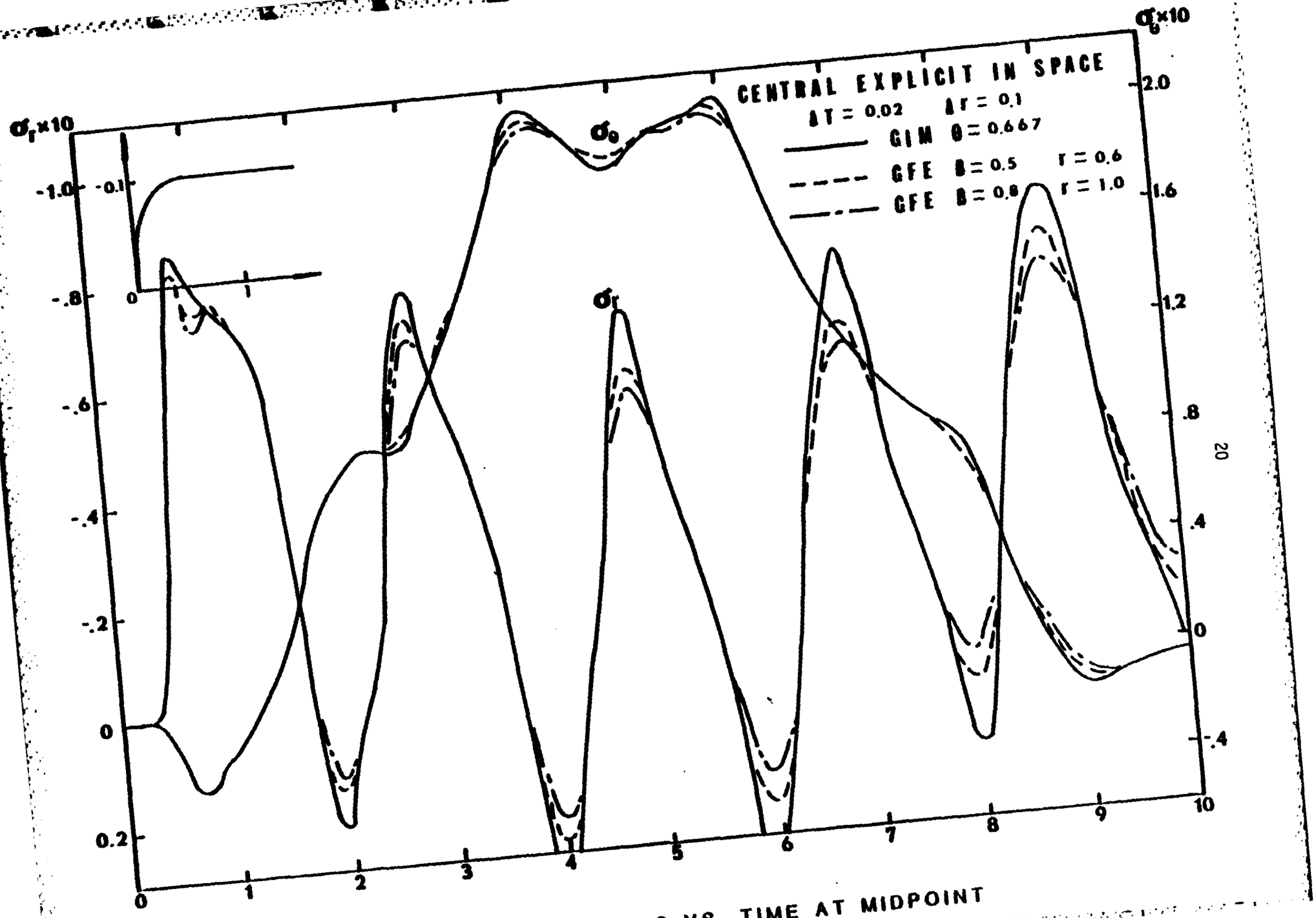

FIG. 6 STRESSES VS. TIME AT MIDPOINT

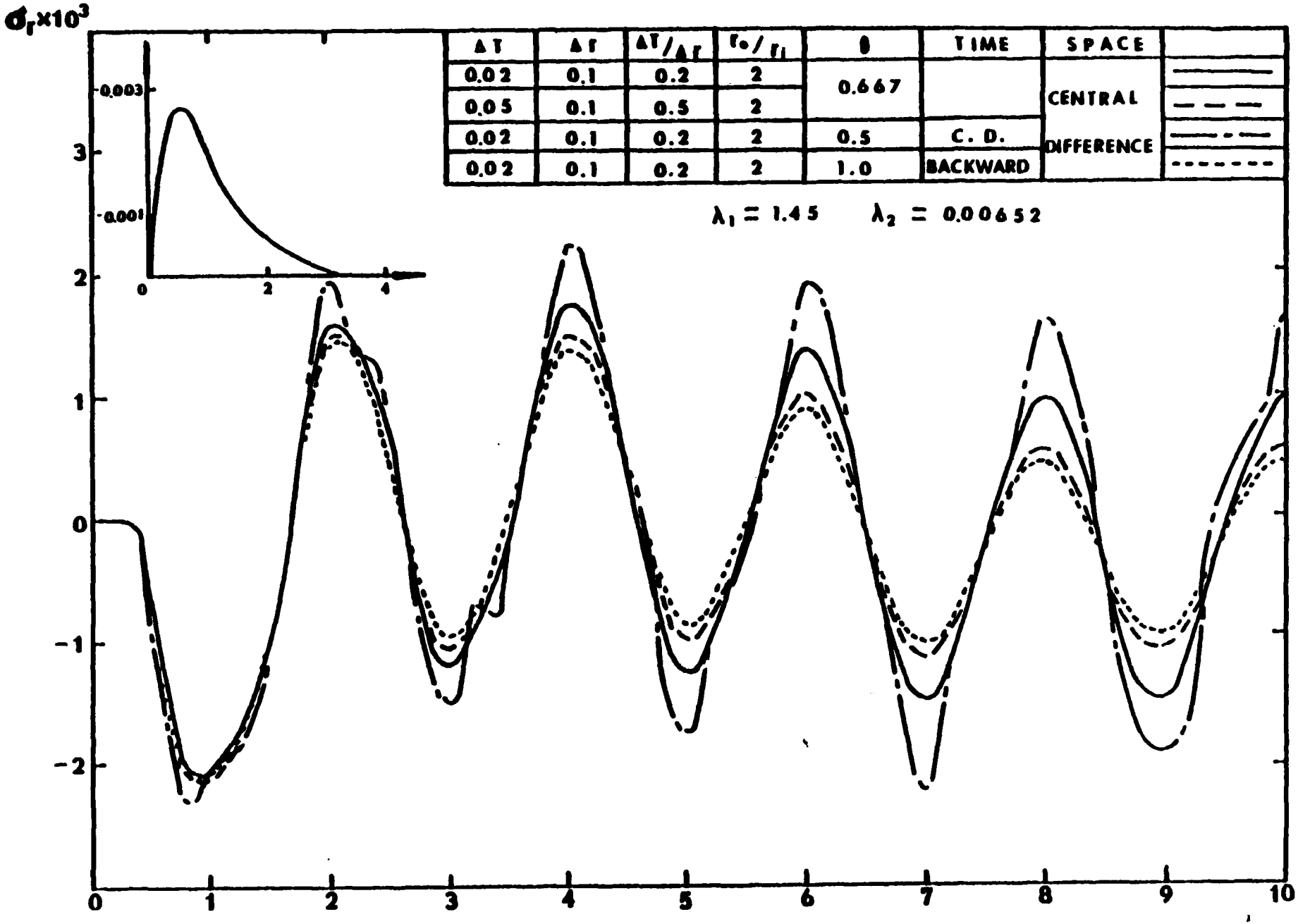

FIG. 7 RADIAL STRESS VS. TIME AT MIDPOINT

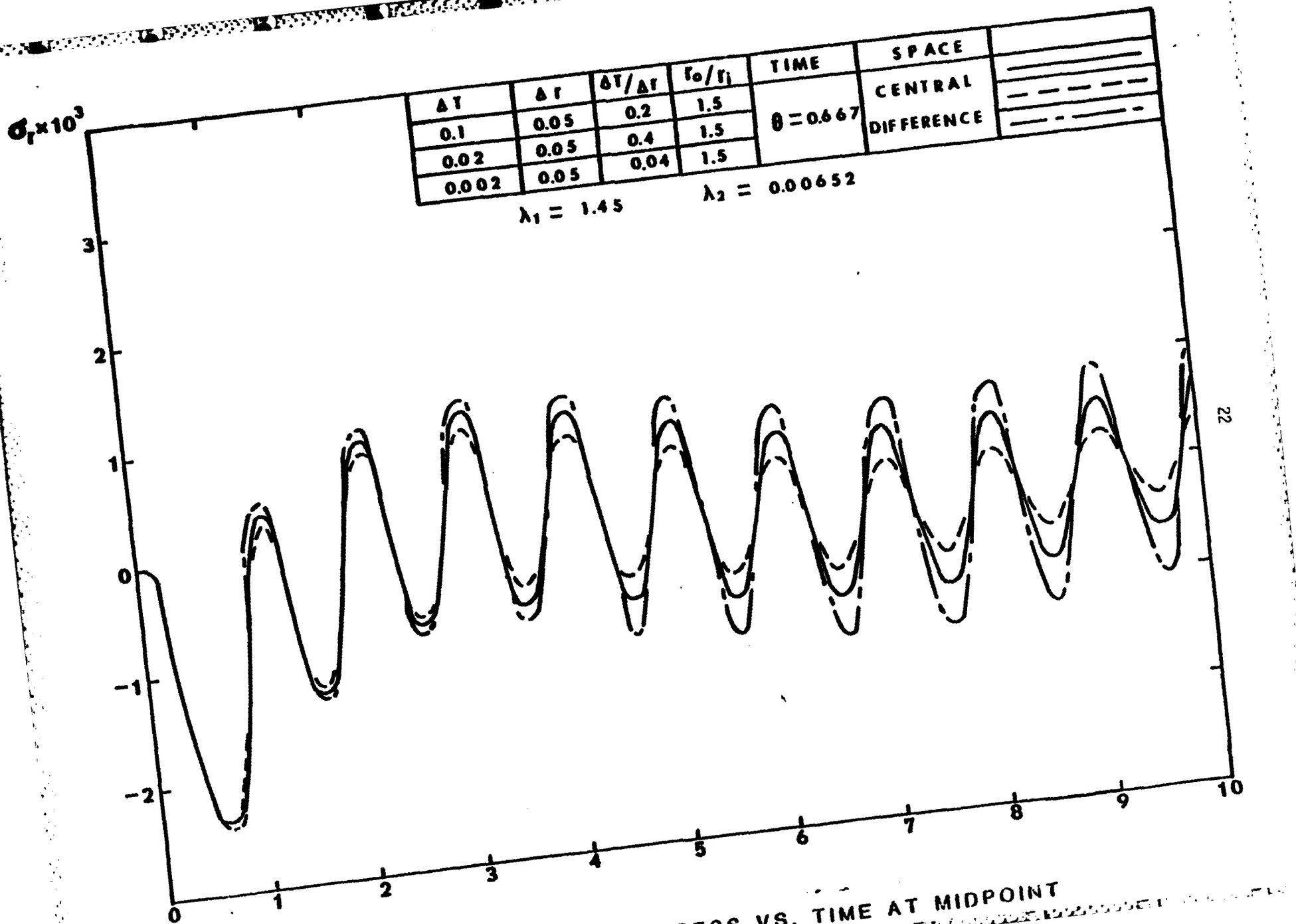

FIG. 8 RADIAL STRESS VS. TIME AT MIDPOINT

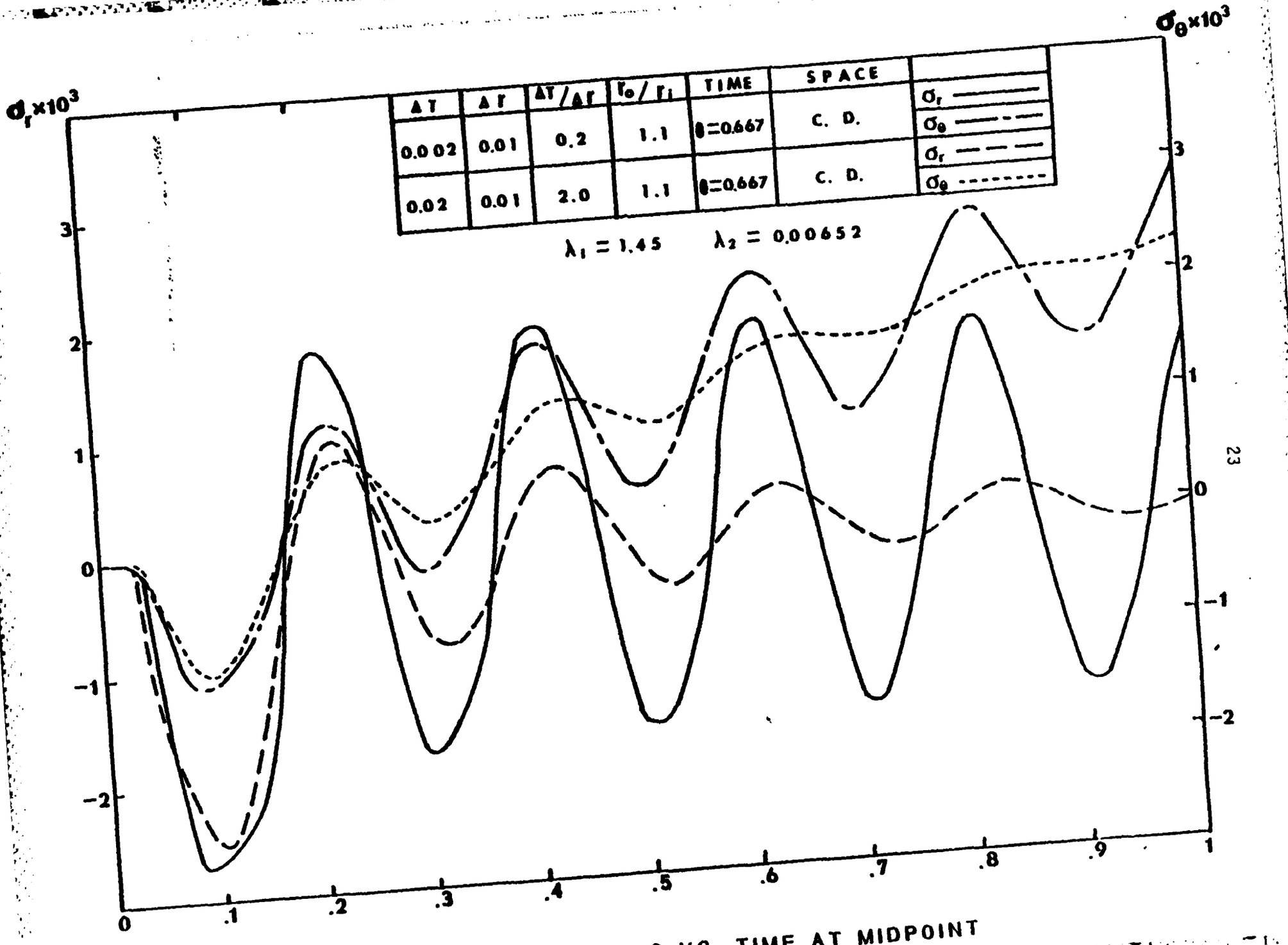

FIG. 9 STRESSES VS. TIME AT MIDPOINT

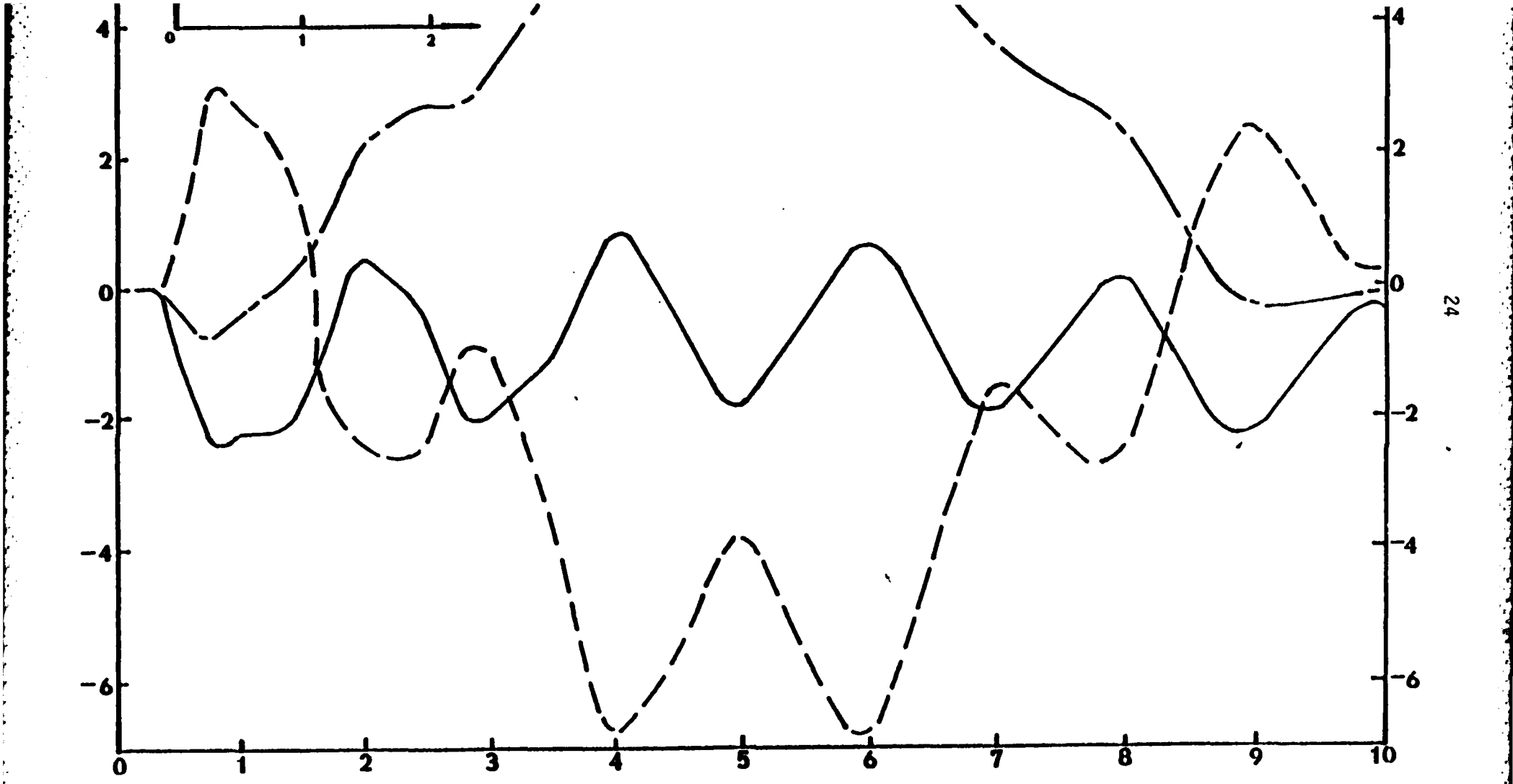

FIG. 10 STRESSES AND TEMPERATURE VS. TIME AT THE MIDPOINT

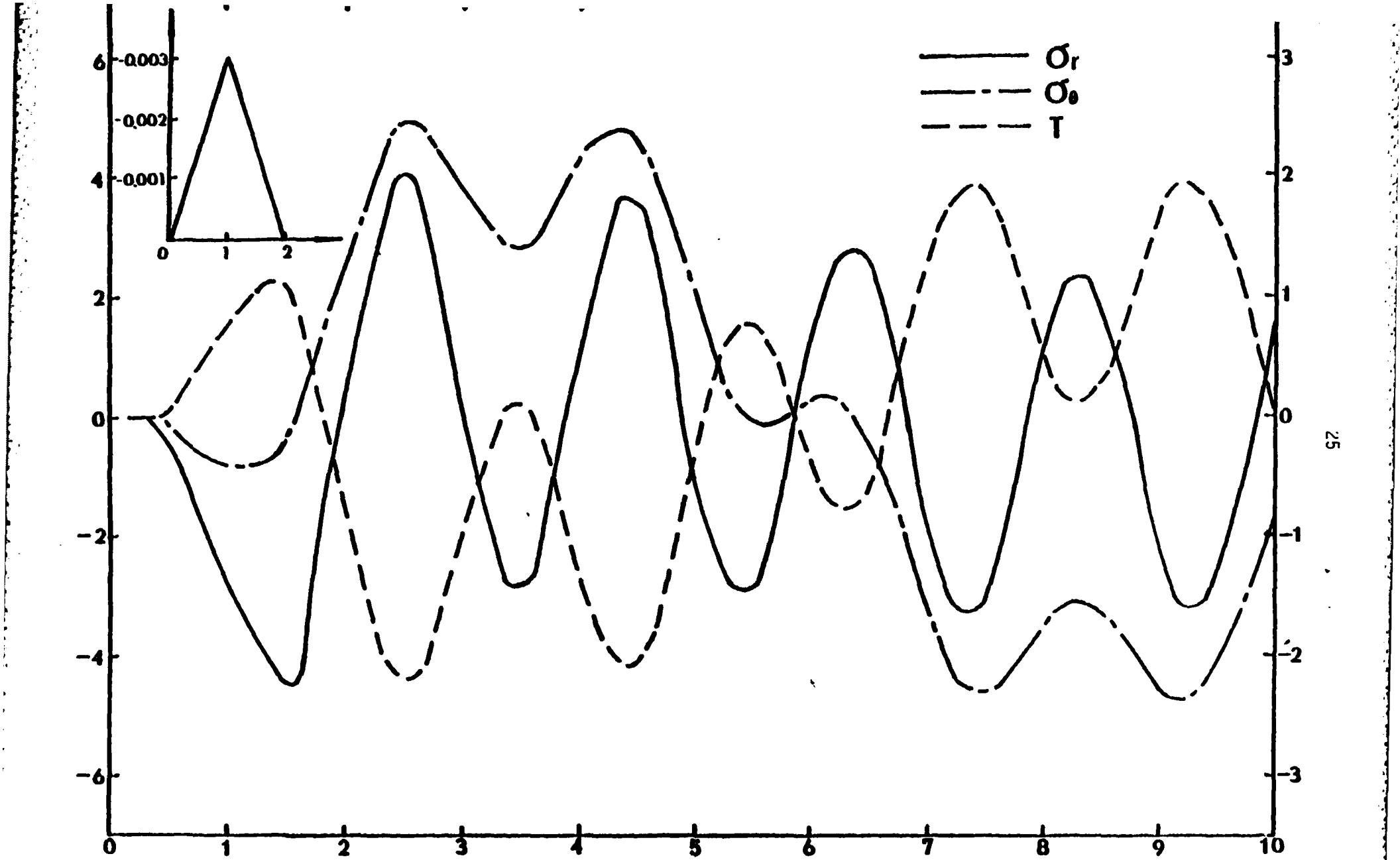

FIG. 11 STRESSES AND TEMPERATURE VS. TIME AT THE MIDPOINT

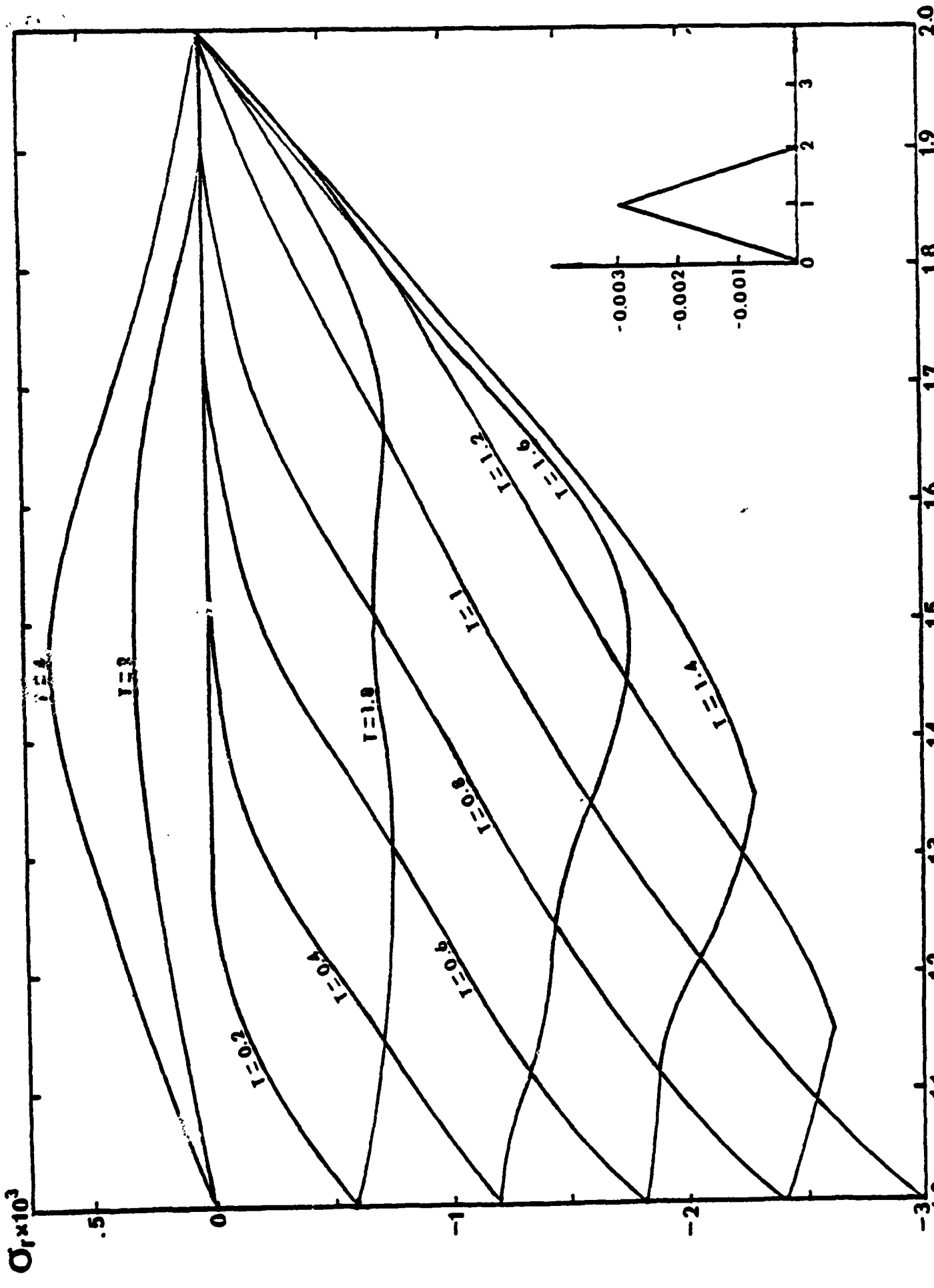

FIG. 12 RADIAL STRESS VS. RADIAL DISTANCE

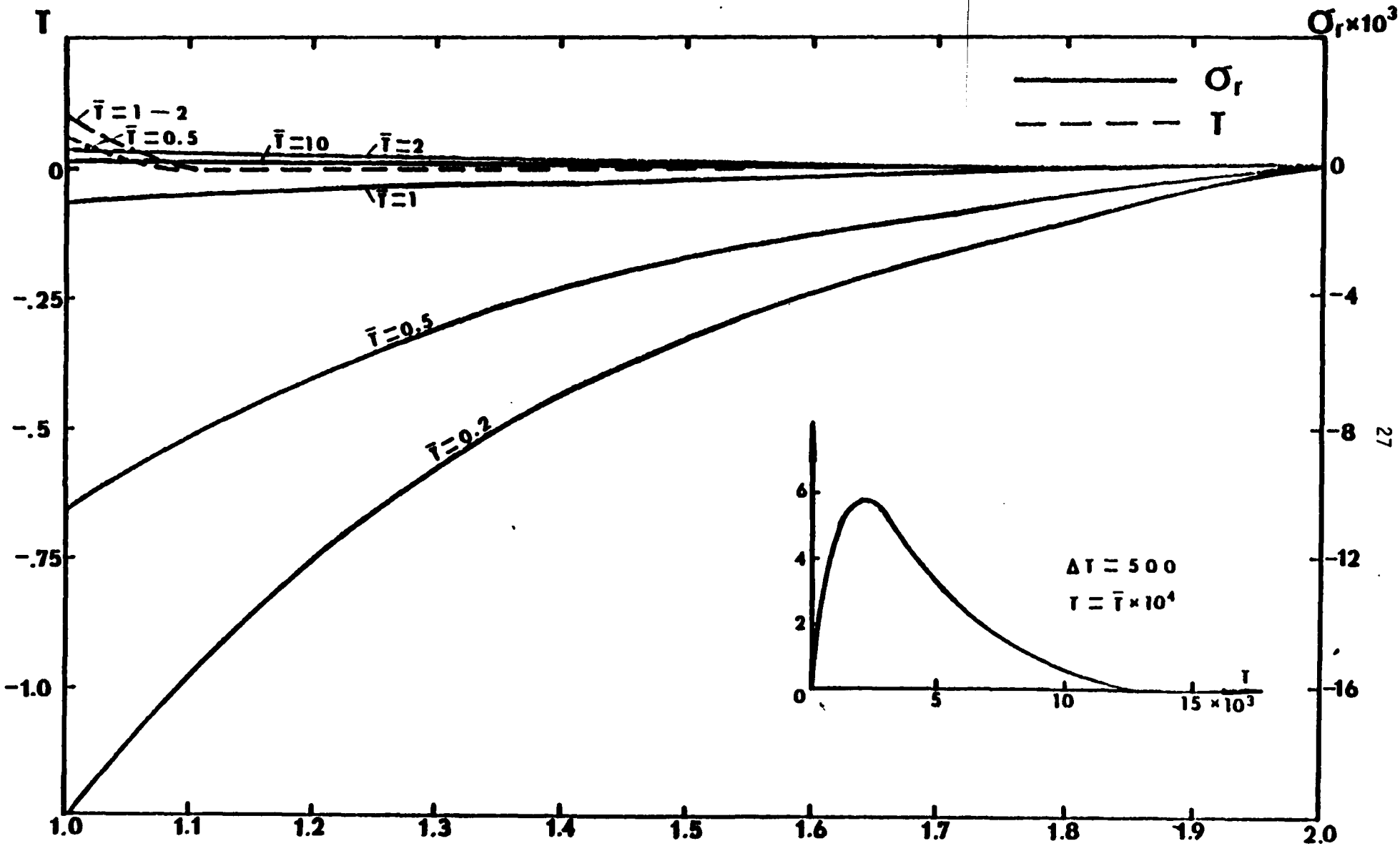

FIG. 13 RADIAL STRESS AND TEMPERATURE VS. RADIAL DISTANCE

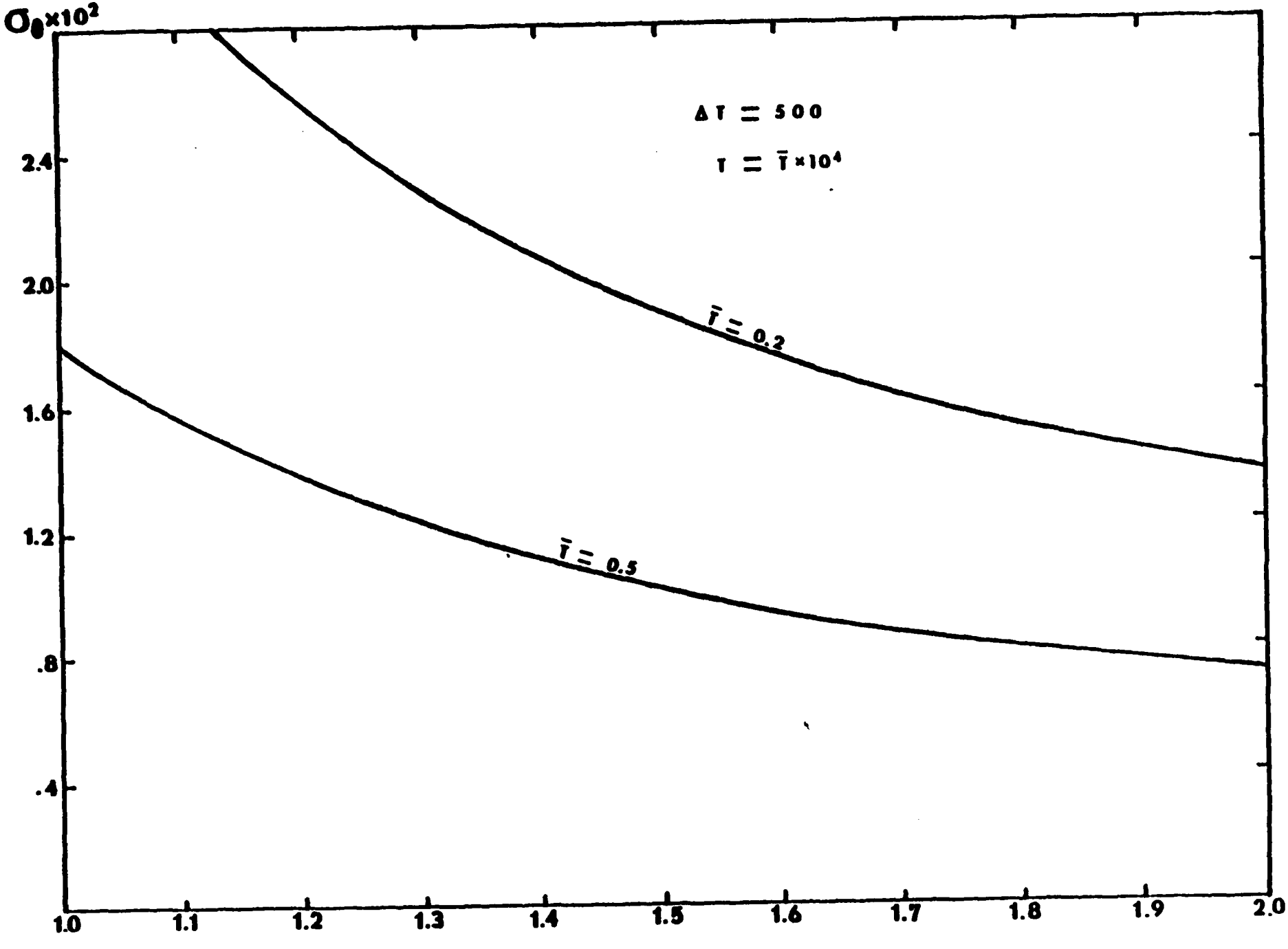

FIG. 14 TANGENTIAL STRESS VS. RADIAL DISTANCE

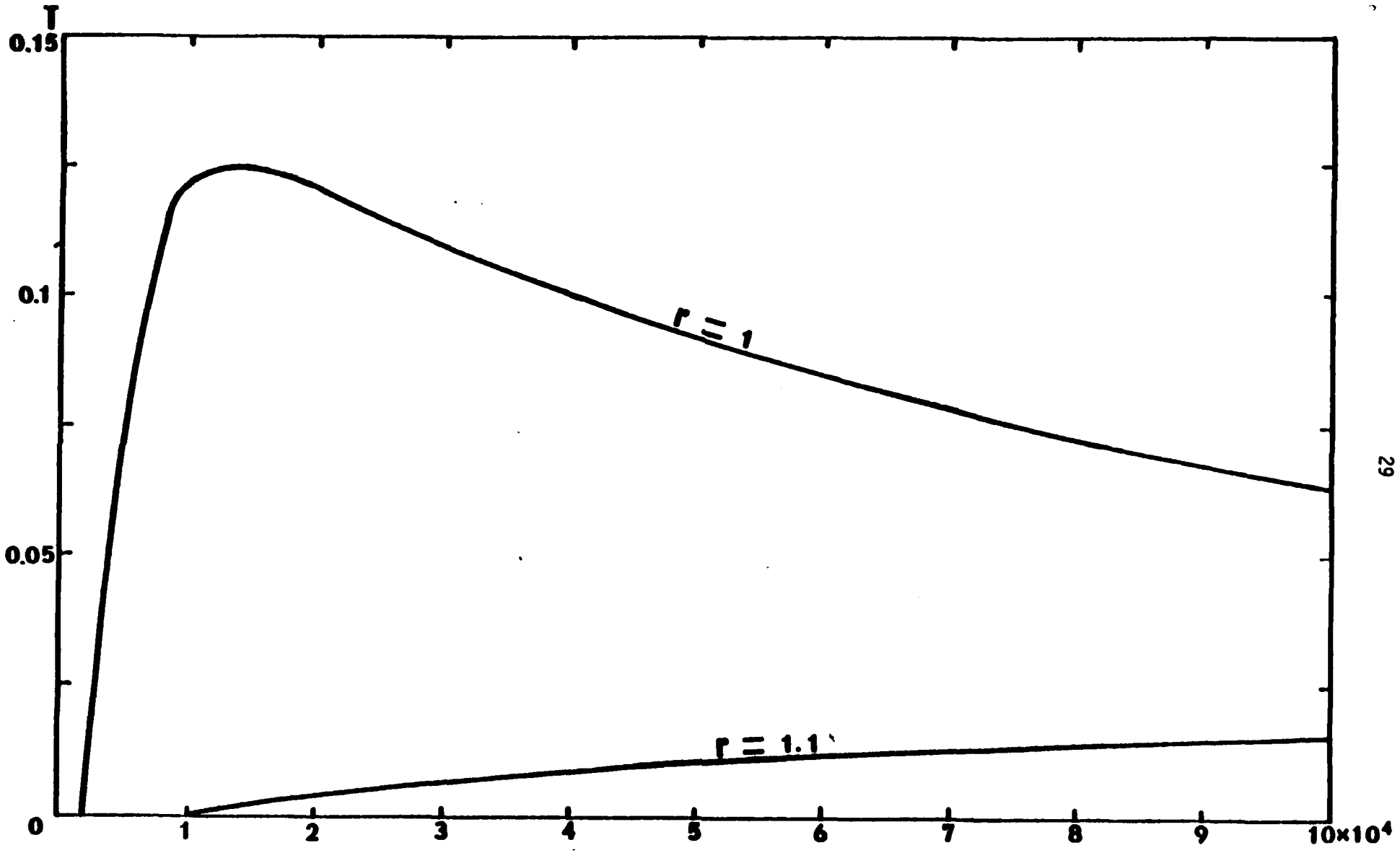

FIG. 15 TEMPERATURE VS. TIME AT TWO RADII

END

FILMED

8-83

DTIC